Studies of ion solitary waves using simulations including hydrogen and oxygen beams

J. P. Crumley, C. A. Cattell, R. L. Lysak, J. P. Dombeck

School of Physics and Astronomy, University of Minnesota, Minneapolis

Abstract. Particle-in-cell simulations of solitary waves have been performed using a 2 spatial and 3 velocity dimension electrostatic code with one electron and two ion species. Data from the Fast Auroral Snapshot (FAST) and Polar spacecraft are used to provide input parameters, and on the basis of these observations, no cold plasma was included in contrast to earlier simulations. Simulations containing both oxygen and hydrogen beams are compared to simulations that contain only hydrogen to examine the effects of the oxygen on the behavior of the solitary waves. In both cases the solitary wave speeds are less than the hydrogen beam speed, and they are also greater than the oxygen beam speed for the cases including oxygen. The simulated solitary waves have spatial scales of the order of 10 λ_D and potential amplitudes of the order of 0.1 $e\phi/kT_e$, which are consistent with Polar spacecraft observations in the low-altitude auroral zone.

1. Introduction

Solitary waves traveling parallel to the background magnetic field have been observed in many parts of the magnetosphere. These solitary structures are identified by their bipolar electric field structure parallel to the magnetic field. First seen in the auroral acceleration region by S3-3 [*Temerin et al.*, 1982], solitary waves have since been observed in many regions of the magnetosphere, including the cusp, bow shock, plasma sheet boundary layer, magnetosheath, and magnetotail. Recent observations of solitary waves in the auroral zone suggest that there are two classes of solitary waves: those associated with electron beams and those associated with ion beams [*Ergun et al.*, 1998]. Solitary waves associated with electron beams tend to have higher speeds than those associated with ion beams. Solitary waves that are associated with ion beams were first observed in the auroral acceleration region by S3-3 [*Temerin et al.*, 1982], later by Viking [*Boström et al.*, 1988], and most recently by Fast Auroral Snapshot (FAST) [*McFadden et al.*, 1999a] and Polar [*Mozer et al.*, 1997; *Bounds et al.*, 1999]. Solitary waves associated with electrons were first observed by Geotail [*Matsumoto et al.*, 1994] and later by FAST [*Ergun et al.*, 1998], Polar [*Cattell et al.*, 1999; *Franz et al.*, 1998, 2000], and Wind [*Bale et al.*, 1998].

S3-3's original observations of solitary waves in the ion beam region had solitary waves with a lower limit of several volts of net potential drop across the structure and a lower limit of 50 km s^{-1} on the speeds of the structures. The structures had sizes both parallel and perpendicular to the background magnetic field of $\sim$ 40 λ_D, assuming that there was a cold background plasma population [*Temerin et al.*, 1982]. Viking's observations gave net potential drops up to 2-3 V and speeds of 5 - 50 km s^{-1}. Scale sizes were of the order of 50-100 m, with the perpendicular scale sizes being slightly greater than the parallel sizes. These scale sizes translated to $\sim$ 10 λ_D, including a cold electron population of 5 eV and 5 cm^{-3} [*Koskinen et al.*, 1990; *Mälkki et al.*, 1993] that was indicated by the Viking observations.

A recent Polar spacecraft statistical study of ion-related solitary waves in the auroral acceleration region [*Dombeck et al.*, 1999] gives much different characteristics for these structures. The potential amplitude of the structures, $e\phi/kT_e$ (where e is the fundamental charge, ϕ is the potential amplitude, k is Boltzmann's constant, and T_e is the electron temperature), is $\sim$ 0.1, where kT_e is up to 1 keV (i.e., potentials of 10-100 V). The solitary wave speeds are between the hydrogen and oxygen beam speeds, in the same 75-300 km s^{-1} range as that found in a previous Polar study [*Bounds et al.*, 1999]. The scale size in the parallel direction is $\sim$ 10-20 λ_D, with the Debye length being $\sim$ 200 m in this case (J. P. Dombeck et al., "Observed trends in auroral zone ion-mode solitary wave structure characteristics using data from Polar," submitted to *Journal of Geophysical Research*, 2001, hereinafter referred to as Dombeck et al., in press, 2001). Recent FAST observations have indicated that cold plasma

Table 1. Simulation Parameters

Parameter	Simulation Value	Physical Value
Grid size	128 by 128	21.2 km by 21.2 km
Size of each grid box	1 λ_D by 1 λ_D	165 m by 165 m
Plasma frequency	1 ω_{pe}	9 KHz
Number of time steps	10,000	
Length of time step	0.3 ω_{pe}^{-1}	33 μs
Electron cyclotron frequency	9 ω_{pe}	81 kHz
Electric field	0.6 T_e/eL_x	14 mV m^{-1}
Hydrogen to electron mass ratio	100	1,836
Oxygen to hydrogen mass ratio	16	16

densities are insignificant in the upward ion beam region [*Strangeway et al.*, 1998; *McFadden et al.*, 1999c]. These observations are the motivation for this study of ion beam related solitary waves.

Previous simulation studies of the ion beam related solitary waves attempting to explain the S3-3 and Viking observations [*Boström et al.*, 1988] have described ion solitary waves as being related to ion acoustic solitons [*Barnes et al.*, 1985; *Marchenko and Hudson*, 1995], or Bernstein-Greene-Kruskal (BGK) ion phase space holes [*Tetreault*, 1991], while electron beam related solitary waves are thought to be electron acoustic waves [*Dubouloz et al.*, 1991], or BGK phase space holes [*Muschietti et al.*, 1999a, 1999b; *Goldman et al.*, 1999; *Singh*, 2000]. The work on ion acoustic solitons is based on the theory that nonlinear, coherent potential pulses can develop from linear acoustic waves [*Lotko*, 1983]. Later work extended this theory to include H^+ and O^+ beams [*Qian et al.*, 1989]. In the simulations these structures developed from the interaction of one or more ion or electron beams with background ion and electron populations. The BGK phase hole theory is based on the idea that holes in the phase space distribution of ions can develop owing to thermal fluctuations, and that these holes can propagate and grow [*Dupree*, 1982]. In simulations these structures form owing to drifts between ion and electron species and owing to thermal fluctuations. Simulations of both mechanisms for developing solitary waves matched the S3-3 and Viking observations fairly well, but the new observations of plasma distributions and solitary wave characteristics suggest the need for new simulation studies.

In this study we examine ion beam related solitary waves seen in the auroral acceleration region. Our goal is to determine the effect of (1) no cold plasma and (2) ion composition, on the solitary waves. The parameters we use are based on FAST and Polar observations of the auroral acceleration region [*Strangeway et al.*, 1998; *McFadden et al.*, 1999c]. In order to model the observed plasma parameters, we include hydrogen and oxygen ions, since both species are usually present in ion beams in the auroral acceleration region. Previous one-dimensional (1-D) studies of solitary waves [*Hudson et al.*, 1987] have shown that the inclusion of both ion species results in the two-stream instability which affects the range of conditions under which solitary waves can form. Further 1-D studies [*Gray et al.*, 1992] showed that solitary waves formed more quickly when oxygen was present than when only hydrogen was included. We will compare the results of our simulations to theories and recent observations of ion solitary waves. In section 2 we describe the details of the simulation. Section 3 presents results of some of the simulation runs. Comparison to observation and a discussion of the significance of our studies are given in section 4.

2. Simulation Details

Our simulations were done using ES2 [see, e.g., *Marchenko and Hudson*, 1995], a 2.5-dimensional, electrostatic particle-in-cell code with periodic boundary conditions. See Table 1 for details on simulation parameters used and the physical values that they correspond to. A 128 by 128 grid was used for the runs presented here, with each grid being one Debye length long on a side. The simulations were run with time steps equal to 0.3 times the inverse electron plasma frequency (ω_{pe}^{-1}), with 10,000 iterations done for each run. In addition, runs were completed with a 1024 by 128 grid and with time steps of 0.03 ω_{pe}^{-1} to examine numerical effects. Potential plots were averaged over 100 iterations (30 ω_{pe}^{-1}) in order to average out high-frequency noise. The plasma was magnetized so that the electron cyclotron frequency was equal to 9 times the electron plasma frequency. The chosen

Table 2. Species-Dependent Parameters

	Electron	Proton	Oxygen
Number of particles	13,1072	65,536	65,536
Temperature (T_e)	1	0.2	0.2
Beam speed (v_{te})	0	0.2-0.8	0.05-0.2

value for the cyclotron frequency leads to a highly magnetized plasma, which previous studies [*Barnes et al.*, 1985] had indicated was necessary for solitary wave formation. An electric field, equivalent to a potential drop of 0.6 T_e across the simulation box, was applied along the magnetic field direction. The applied electric field is added to simulate the field-aligned potential drop seen in the auroral acceleration region, as has been done in previous particle-in-cell (PIC) studies of solitary waves [*Marchenko and Hudson*, 1995]. This electric field accelerates the particles and results in relative drifts which provide the source of free energy for the solitary waves.

Simulations of both two- and three-species plasmas are presented here. In the two-species cases the plasma species used are a stationary hot electron population and a hydrogen beam (with the physical number density of each being 1 cm^{-3}). In the three-species cases an oxygen beam is added. A study of ion beam events in the auroral zone using FAST [*McFadden et al.*, 1999c] data found that the ratio of O^+ number density to H^+ number density ranged from 0.28 to 1.44, with typical values being around 1. *McFadden et al.* [1999c] also found that the ratio of He^+ number density to H^+ number density ranged from 0.20 to 0.67, so helium ions could also play a role in the dynamics of ion-associated solitary waves. For the purposes of this study it was decided that looking only at hydrogen and oxygen beams would be sufficient. Future studies will also include helium. The oxygen to hydrogen number density ratio of 1 was chosen since it is fairly typical of the observations. *McFadden et al.* [1999c] also found plasma sheet ion densities which ranged from much smaller than the beam densities up to comparable densities. For the purposes of this study we choose to ignore the plasma sheet population, though future studies will include it.

The ion beams start out with equal energies, giving them different velocities, which leads to two stream interactions between the beams [*Bergmann et al.*, 1988]. Simulations were run with the ratio of hydrogen to electron mass equal to 100 to conserve computing time [*Barnes et al.*, 1985], while the oxygen to hydrogen mass ratio was 16. The plasma species parameters for the three-plasma species cases are shown in Table 2 and were chosen to follow the parameters recently observed [*McFadden et al.*, 1999c]. The parameters used for the two-species cases are identical, except that all of the oxygen particles are replaced by hydrogen. In the simulations all values are normalized, and the physical units matching these choices were as follows. The electron temperature was initially 0.5 keV, while both ion species had temperatures of 0.1 keV. The ion beams were chosen to have drift energies ranging from 2 to 32 keV. Some of these drift energies are higher than the range from 0.8 to 10 keV seen by FAST [*McFadden et al.*, 1999c], but the higher values were used so that there would be a wider range over which to determine the effects of changing the beam energy.

3. Simulation Results

Results of a simulation with a hydrogen beam of speed 0.4 v_{te} and an oxygen beam speed of 0.1 v_{te} are shown in Plate 1, where v_{te} is the electron thermal speed. The solitary waves can be identified as nearly circular depressions in the electrostatic potential in these simulations (see Plates 1e and 1f). At the beginning of a simulation run, the potential is flat, but electrostatic ion cyclotron wave perturbations in the potential begin to build up. These perturbations occur at both the hydrogen and oxygen cyclotron frequencies. Solitary structures begin to form after $\sim$ 400 ω_{pe}^{-1}. They propagate in the beam direction and last between 150 and 2000 ω_{pe}^{-1}, with typical lifetimes of $\sim$ 400 ω_{pe}^{-1}. The solitary structures are circular in shape with radii of the order of 10 λ_D. The size of the structures changes during their lifetime, with a typical solitary wave starting out small both in amplitude and spatial size, growing for a time, then shrinking, and dissipating. The shapes vary somewhat between solitary waves in the same run, with the shapes having a range of oblateness, but with a definite tendency toward being slightly oblate perpendicular to the magnetic field as in Plates 1e and 1f. This leads to typical scale sizes being slightly larger in the perpendicular direction ($\sim$ 15 λ_D).

The development of the solitary structures is also evident in the phase space densities of the plasma species (see Plates

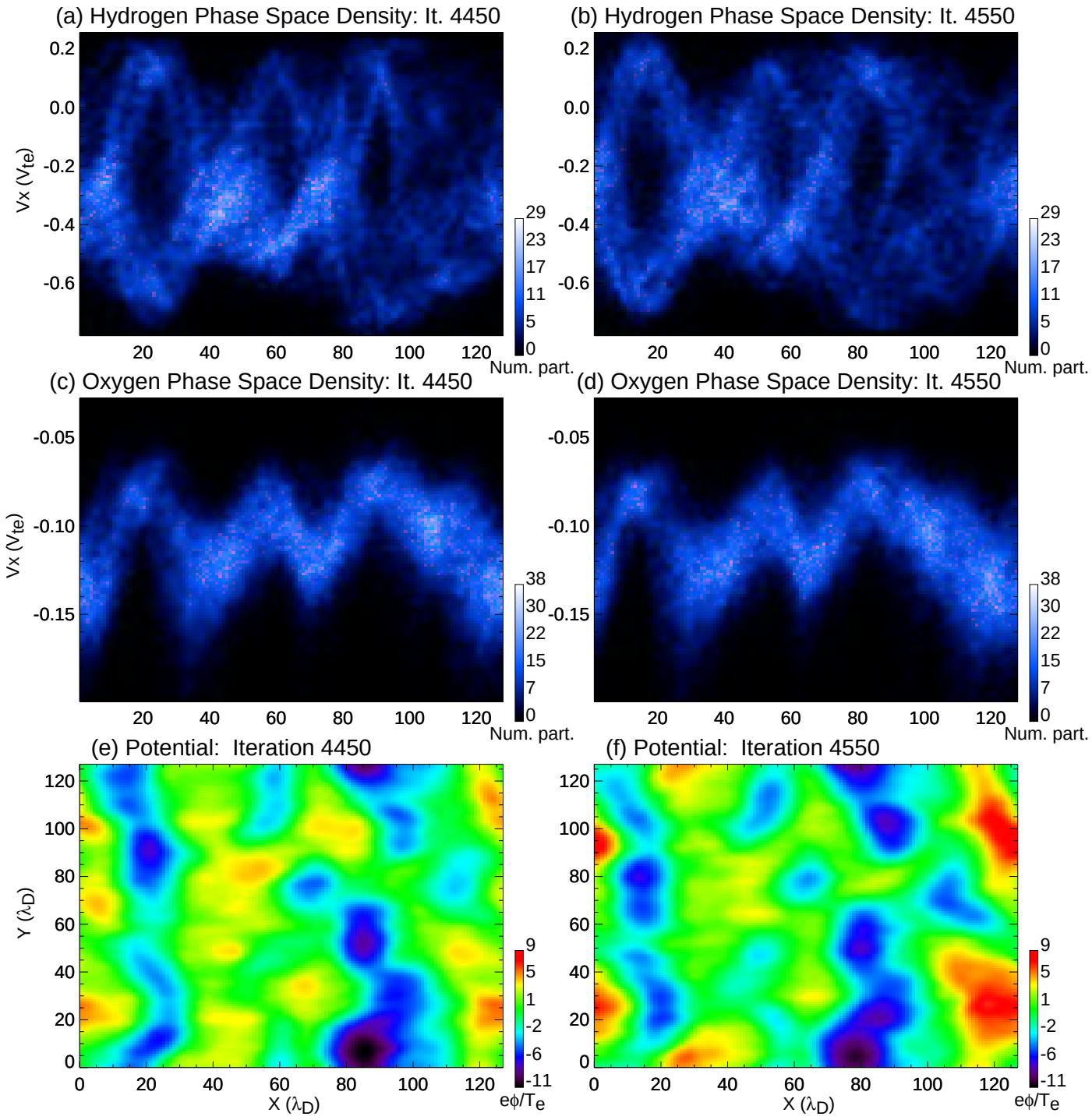

Plate 1. Phase space densities for (a,b) the hydrogen ions and (c,d) the oxygen ions, as well as (e,f) the electrostatic potential, for iterations 4450 (1335 ω_{pe}^{-1}) and 4550 (1365 ω_{pe}^{-1}). The electrostatic potential are in units of kT_{e_0}/e, where T_{e_0} is the original electron temperature. The phase space density plots are in particles per phase space grid box, where the phase space grid is divided into 128 in the *X* direction and 100 in the V_X direction. These plots are from the 8-keV beam run, which corresponds to beam speeds of 0.4 v_{te} and 0.1 v_{te} for the hydrogen and oxygen beams, respectively. The electrostatic potential shown is averaged over 100 iterations (30 ω_{pe}^{-1}) to remove high-frequency oscillations. The solitary waves are the dark, circular areas of negative potential, and they move from right to left with ion beams. This is the same direction as the ion beams and applied electric field and the opposite direction from the background magnetic field.

1a-1d). Initially, all species are Maxwellians, but the distributions begin to show sizeable fluctuations at about the same time that solitary structures first appear in the potential. These fluctuations tend to be in phase spatially between species, with the major peaks and troughs of the phase space density tending to line up across species. These fluctuations move in the ion beam direction, as the potential structures do. As the simulation progresses, the phase space fluctuations become more pronounced. The simple sinusoidal forms of the early fluctuations are replaced by more complicated forms. The two-stream instability leads to an interesting phase space structure in the hydrogen ions (see Plates 1a and 1b), with a pattern resembling a standing wave. At the antinodes there is a peak in both the negative and positive sides of the velocity axes in the phase space density at the same x value, with a hole in the phase distribution between. At the nodes the phase density reaches its highest values, and particles are spread over a smaller range of speeds. We believe this complex pattern is caused by the balance of the two-stream interaction which tends to bring the hydrogen drift speed down to the oxygen drift speed, and the electric field which tends to accelerate the hydrogen ions more quickly than the oxygen ions. Phase space densities of this type are seen only in the three-species cases. In the two-species cases the hydrogen phase space densities resemble those seen in the oxygen phase space density shown in Plates 1c and 1d. No standing wave patterns are formed in these cases, though sinusoidal phase space oscillations do occur. It is likely that the extra complexity seen in the three-species cases is due to the two-stream interaction.

The effect of the two-stream interaction is evident in the behavior of the ion species drift speeds, as shown in Figure 1. The momentum transfer between the ion species is evident in the sharp fall in the hydrogen drift speed and the rise in the oxygen drift speed centered around iteration 4000 (1200 ω_{pe}^{-1}). This time period is also when the solitary wave activity is greatest. Though the two-stream instability works to equalize the beam speeds of the two ion species, the applied electric field prevents the complete equalization. After iteration 5000 (1500 ω_{pe}^{-1}) the solitary wave activity begins to dissipate, the effects of the applied electric field dominate, and both ion species increase their drift speeds. As with the drift speeds, the effects of the solitary waves are also evident in the parallel (Figure 2) and perpendicular (Figure 3) drift energies of the plasma species. The ion species both have peak heating rates parallel to the magnetic field around iteration 4000, owing to the interaction of the ions with the solitary waves. After the solitary waves dissipate, the parallel thermal energies of the ion species level off, and the hydrogen ions even cool slightly. The electron heating rate is more constant, though the heating rate does peak when

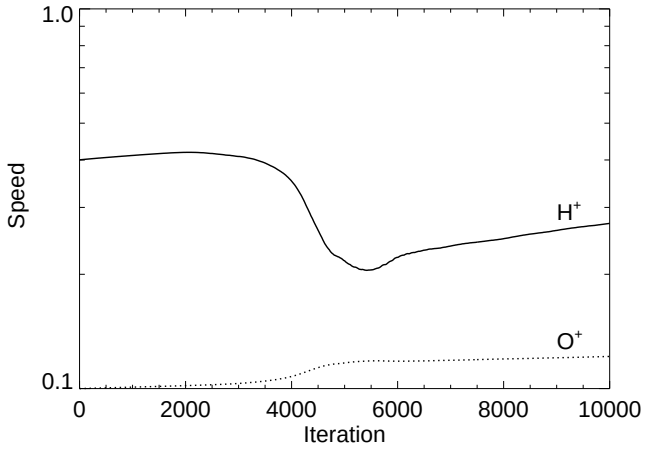

Figure 1. Plot showing the ion drift speeds, with a logarithmic scale in units of the initial electron thermal speed (v_{te}), versus iteration, where each iteration is 0.3 ω_{pe}^{-1}. Figure 1 is for the case where the initial hydrogen drift speed was 0.4 v_{te} and the initial oxygen drift speed was 0.1 v_{te}.

the solitary waves are dominant. The heating rate perpendicular to the magnetic field for the ions also peaks while the solitary waves are dominant (Figures 3b and 3c). The ions show the effects of ion cyclotron waves, with oscillations at the corresponding ion cyclotron frequency evident in both ion species. The electrons show very little heating in the perpendicular direction because the time step size of 0.3 ω_{pe}^{-1} does not resolve oscillations of the order of the electron cyclotron period, $\sim 0.1\ \omega_{pe}^{-1}$.

Some of the physical parameters used for the runs presented here were varied in other runs to examine their effects on the results. The applied electric field was varied, in order to see how it affected the solitary waves. Solitary waves do not develop in this simulation if the field is omitted. Decreasing the value used for the electric field increased the length of time it took for the solitary waves to develop and decreased the potential drop seen in the solitary waves. Utilizing $\Omega_{ce}/\omega_{pe} = 9$ leads to a highly magnetized plasma, which previous studies [*Barnes et al.*, 1985] indicated was necessary for solitary wave formation. To test whether this was the case when there was no cold plasma, several runs with lower magnetic fields (i.e., $\Omega_{ce} = 1\ \omega_{pe}$ and $0.1\ \omega_{pe}$, compared to the original value of $9\ \omega_{pe}$) were done. These runs still had solitary waves, though they were smaller in potential amplitude and slightly more oblate in the perpendicular direction.

Several computational parameters were varied in order to isolate any numerical effects on the simulated solitary waves. Additional runs were performed with grid sizes up

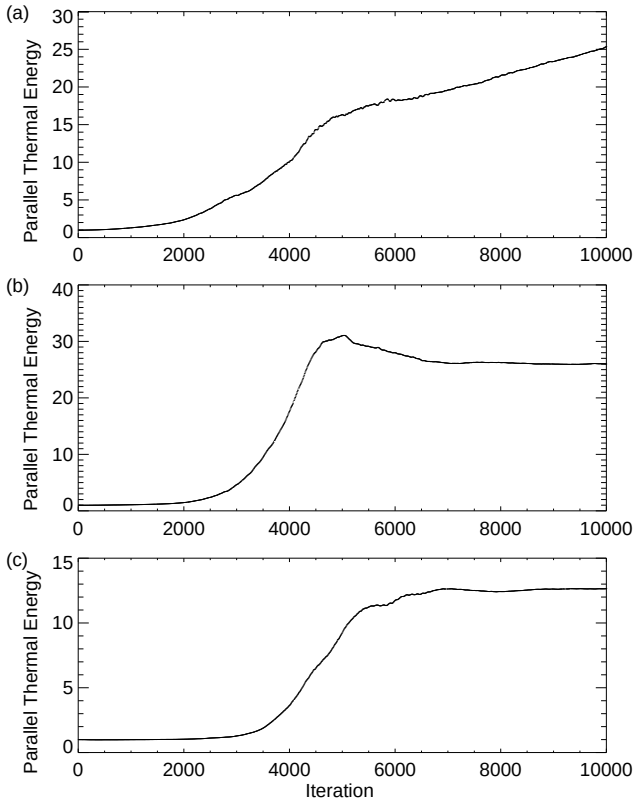

Figure 2. The parallel thermal energy, normalized to the species initial thermal energy, versus iteration, where each iteration is 0.3 ω_{pe}^{-1}, shown for the (a) electrons, (b) hydrogen ions, and (c) oxygen ions. Figure 2 is for the case where the initial hydrogen drift speed was 0.4 v_{te} and the initial oxygen drift speed was 0.1 v_{te}.

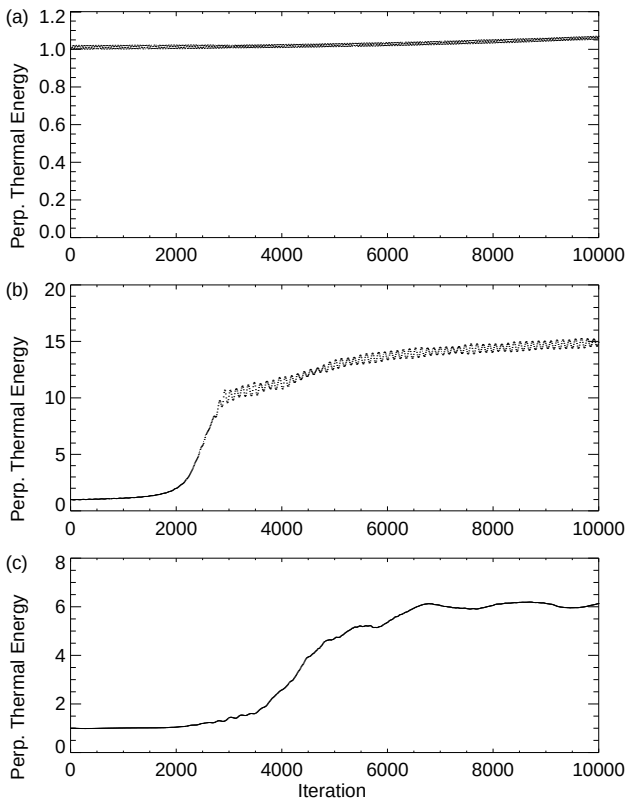

Figure 3. The perpendicular thermal energy, normalized to the species initial thermal energy, versus iteration, where each iteration is 0.3 ω_{pe}^{-1}, shown for the (a) electrons, (b) hydrogen ions, and (c) oxygen ions. Figure 3 is for the case where the initial hydrogen drift speed was 0.4 v_{te} and the initial oxygen drift speed was 0.1 v_{te}.

to 1024 λ_D along the magnetic field line to ensure that particle recycling due to the periodic boundary conditions did not alter the results. These runs gave results which were equivalent to those shown here. The effects of the time step size were also tested by using a time step that was a factor of 10 smaller in one case (0.03 ω_{pe}^{-1} instead of 0.3 ω_{pe}^{-1}). This change had no noticeable effect on the solitary wave behavior, though electrons did heat more in the perpendicular direction than in Figure 3a, since this time step size resolved the electron cyclotron timescale. The effects of the number of simulation particles per grid cell were also tested by performing a simulation run with 8 times as many particles per grid cell. The behavior of the solitary waves was not changed in this run, though there was a decrease in noise which allowed for averaging over fewer iterations.

In order to see how the solitary wave behavior varied with ion beam characteristics, simulation runs were performed for a range of ion beam energies, which were equivalent to initial hydrogen beam drift speeds between 0.2 and 0.8 v_{te}. The speeds at the lower end of this range are more typical of what is observed in the auroral region, but a wide range of drift speeds was examined in order to study the relationship between beam drift speed and solitary wave speed. Runs with this range of beam energies were made with hydrogen and oxygen beams (see Figure 4a), as well as just hydrogen beams (see Figure 4b), in order to assess the effects of the oxygen beam on the solitary waves. The speeds of the solitary waves were determined by following the minimum potential of a structure between iterations to determine how far the structure moved. The solitary wave structures are not always symmetrical, so the minima of the potential do not always fall at the location that is the center of the structure. This leads to uncertainty in the solitary wave speeds, which necessitates averaging the speeds over several frames of the electrostatic potential, or at least 150 ω_{pe}^{-1}, in order to get accurate speeds. These average speeds for each solitary wave are then averaged for a few separate solitary waves to find typical speeds for a run, and they are plotted against beam speeds in Figure 4. The average solitary wave speeds for all runs lie below the hydrogen beam speed. In the cases with both hydrogen and oxygen the solitary wave speeds are between the two beam speeds. This result matches what has been observed by the Polar spacecraft in the auroral acceleration region. *Bounds et al.* [1999] found, using Hydra ion distribution data and assuming that both H^+ and O^+ had equal energies, that the solitary waves had speeds between the beam speeds of H^+ and O^+. Further Polar spacecraft studies found (Dombeck et al., in press, 2001), using H^+ and O^+ distribution data, that the ion solitary waves had speeds between the measured H^+ and O^+ beam speeds.

The electrostatic potential amplitude also shows depen-

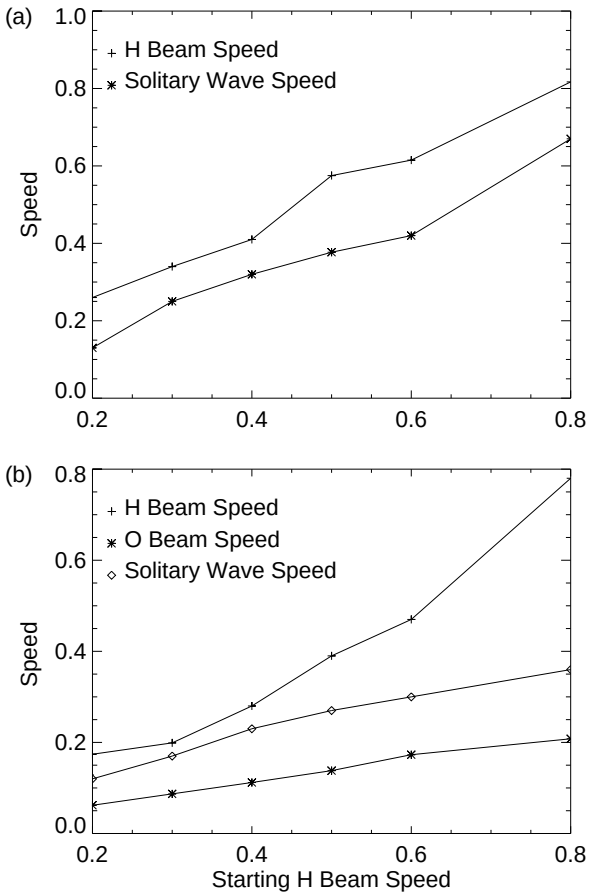

Figure 4. Plots showing solitary wave speeds and beam speeds at the time of the measured solitary waves versus starting hydrogen beam speed for (a) hydrogen beam only runs and (b) hydrogen and oxygen beam runs. All speeds are normalized to the starting electron thermal speed. The beam speeds plotted are taken from the time when the solitary waves are present in the simulations. The beam speeds change during the simulation runs owing to interaction with the other species and with the applied electric field.

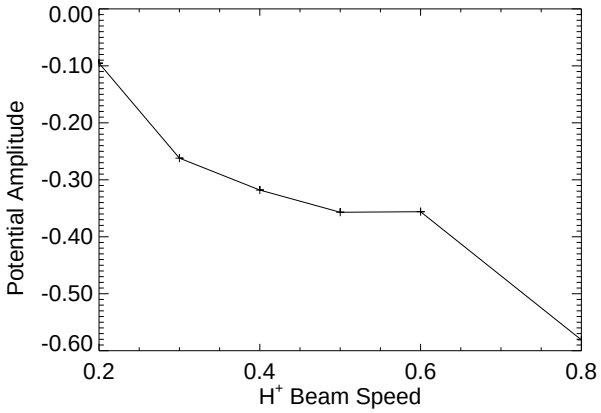

Figure 5. The electrostatic potential amplitude, in units of kT_e/e, versus starting hydrogen beam velocity, in units of v_{te}, plotted for each of the two beam cases that are plotted in Figure 4a. The electrostatic potential amplitudes plotted are the average amplitudes that developed for one solitary wave studied in each run, and they are normalized by the electron temperature at the time the solitary waves were present.

dence on the initial beam energies, as shown in Figure 5. The dependence shown is basically linear, though there is scatter. The scatter is to be expected since the plotted potential amplitudes are the average amplitude of a particular solitary wave for a given simulation run. The general trend of having larger amplitudes when larger beam speeds are used can be explained by the greater free energy made available by the more energetic beams, which is converted into electrostatic potential energy by the solitary structures.

4. Discussion

4.1. Comparison to Theory

We have presented new results on ion solitary structures which differ from previous studies because the plasma parameters in the simulation are based on recent Polar and FAST data. The absence of cold plasma and the inclusion of oxygen ions distinguish this work from previous studies [*Barnes et al.*, 1985; *Marchenko and Hudson*, 1995]. Previous 1-D simulations which included cold plasmas and one ion beam found that solitary waves can form from linear ion acoustic waves that are pumped by the decay of ion beam modes [*Gray et al.*, 1991]. In our H^+ beam cases similar processes may be occurring, with the hot electrons providing the background population in place of the cold plasma. For the H^+ and O^+ beam cases, comparison with studies including both species is enlightening. Linear analysis of H^+ and O^+ beams of equal energies showed that two-stream instabilities can excite modes that propagate both parallel to [*Bergmann and Lotko*, 1986] and oblique to [*Bergmann et al.*, 1988] the background magnetic field. The modes excited by the two-stream instability are related to the acoustic and cyclotron modes of hydrogen and oxygen. The 1-D simulation studies including cold H^+ and O^+ beams found that the ion two-stream instability led to ion acoustic turbulence which grew nonlinearly into solitary waves [*Gray et al.*, 1992]. Similar processes are at work in the H^+/O^+ beam cases presented here, so that the solitary waves from both H^+ and H^+/O^+ cases are likely being formed from ion acoustic turbulence, and we classify these structures as "ion acoustic solitary waves." The term "ion acoustic solitary wave" is used instead of "ion acoustic soliton" because it is not clear that these structures meet the strict mathematical definition of the term "soliton."

The propagation speeds of the solitary waves in this study fit reasonably well with theory. Ion acoustic soliton theory predicted that the solitons should have a velocity equal to the ion acoustic speed relative to the reference frame of the cold ion species [*Lotko*, 1983], which is the same as the phase velocity of linear ion acoustic waves. This idea was later extended to allow for the replacement of the cold background population by an ion beam of another species [*Qian et al.*, 1989]. When this theory was applied to simulation studies, it was found that the solitary structures slow down as their amplitude increases [*Hudson et al.*, 1983]. So the difference between the speed of the solitary waves and the population they are riding on is expected to be less than the ion acoustic speed. Applying these principles to the H^+ beam case, it would be expected that the solitary waves would move with a speed somewhat less than 0.1 v_{te} slower than the hydrogen beam speed, since the hydrogen acoustic speed is 0.1 v_{te}. From Figure 4a it can be seen that the speed difference between the solitary waves and the hydrogen beam is of the order of the hydrogen acoustic speed, but for the higher speed beams the difference tends to be substantially greater than 0.1 v_{te}. The speed discrepancies for high initial beam speeds may be a result of the fact that the electrons are heated during the simulation, with this heating being more pronounced in the higher beam speed cases, which causes an increase of the hydrogen acoustic speed from its starting value. The solitary wave speeds in the H^+ and O^+ beam cases are also consistent with describing the structures as ion acoustic solitary waves. The speeds of the solitary waves are between the beam speeds of hydrogen and oxygen beams, as would be expected since the most linear modes are in this region [*Bergmann et al.*, 1988]. Some shift in the phase velocities is expected in the context of these nonlinear simulations, but a reasonable first approximation is to expect that the solitary

structures will propagate at speeds about equal to the hydrogen acoustic speed relative to one of the beam species. As shown in Figure 4b, for low beam speeds, the solitary wave speeds relative to the hydrogen beam speed are less than 0.1 v_{te}, while for the higher beam speeds they are much more than 0.4 v_{te}. The solitary wave speed and the oxygen beam speed lines track each other more closely, so it is possible that the solitary structures are hydrogen modes riding on the oxygen beam, instead of the hydrogen beam. This result is consistent with speculation that a second ion species could take the place of a cold background ion population [*Cattell et al.*, 1999]. The 0.05 - 0.15 v_{te} between the oxygen beam and the solitary waves is very similar to the velocity differences seen between the hydrogen beam and the solitary structures in the H^+ beam case.

The parallel scale sizes for the observed solitary waves are consistent with ion acoustic soliton theory. The scale sizes seen here were $\sim$ 10 λ_D in both directions. From *Zakharov and Kuznetsov* [1974] it is expected that these solitary waves would have scale sizes $\sim$ 10 λ_D parallel to the magnetic field and $\sim 10\sqrt{{\lambda_D}^2 + {\rho_H}^2} \approx 15\ \lambda_D$ perpendicular to the magnetic field for these simulations, where ρ_H is the hydrogen ion gyroradius. *Marchenko and Hudson* [1995] pointed out that care must be taken when comparing scale size results to observations in cases like this when an artificial electron to proton mass ratio is used. The artificial mass ratio affects the expected scale size ratio, with results for a physical electron to proton mass ratio being 3.2 times higher, yielding an expected perpendicular scale size of $\sim$ 50 λ_D, in this case. So, if the solitary structures in these simulations were ion acoustic solitons, it would be expected that the physically observed solitary structures would be much larger in the perpendicular direction than in the parallel direction. Another important consideration is that since the potential is averaged over time, the parallel size of the solitary waves may be exaggerated owing to the motion of the solitary waves along the magnetic field.

In contrast to previous results, solitary waves formed for cyclotron frequencies less than the electron plasma frequency, [*Barnes et al.*, 1985; *Marchenko and Hudson*, 1995]. The difference in plasma parameters probably explains this discrepancy. The earlier work did not include O^+ and did include cold plasma, which had a smaller gyroradius.

Since a cold background population was required to support BGK ion phase space holes in formulations where thermal fluctuations are invoked as a generation mechanism [*Tetreault*, 1991], it is unlikely that the solitary waves shown herein are BGK phase space holes of that type. Although it is possible that the oxygen beam could act as a cold population for the hydrogen beam, this would still not explain the structures seen in the hydrogen-only beam case. So we believe that it is unlikely that the structures we see are BGK ion phase space holes caused by thermal fluctuations in cold plasma. However, the results for the H^+ and O^+ beam cases do show structures that appear to be phase space vortices. It is possible that the structures that we see are BGK phase space holes that have been generated by the two-stream interaction, by ion acoustic waves, or by ion cyclotron waves. Further comparisons to expected BGK mode characteristics will be included in an upcoming study.

4.2. Comparison to Observations

The solitary waves observed in the simulations described herein are in agreement with recent Polar observations on a number of points. The speeds of the simulated solitary waves presented here are intermediate between the O^+ and H^+ beam speeds, consistent with those seen by Polar (Dombeck et al., in press, 2001). This result is in contrast to previous simulation studies of ion-related solitary waves, including cold plasma [*Marchenko and Hudson*, 1995], which resulted in much lower speeds. These lower speeds are not surprising, since there was a cold population to support them, and speeds of the order of bulk velocity or beam velocities would be expected when there is no cold plasma present. The speeds found in those simulations matched the observational results of *Boström et al.* [1988] from Viking which gave the solitary wave speeds as being between 5 and 50 km s^{-1}, much less than the ion beam speed. Note that recent FAST observations found that some of the highest amplitude solitary waves had speeds above the hydrogen beam speed [*McFadden et al.*, 1999b]. This is not observed in our simulations. The size of the simulated ion solitary structures, $\sim$ 10 λ_D parallel to the magnetic field, is also consistent with the structure sizes seen by Polar [*Bounds et al.*, 1999; Dombeck et al., in press, 2001]. Although scale sizes perpendicular to the magnetic field have not been observed in as much detail, owing to difficulties in determining sizes transverse to the direction of the motion, preliminary results (Dombeck et al., in press, 2001)suggest that the scale size in the perpendicular direction is slightly larger ($\sim$ 15 λ_D) than in the parallel direction. This result contradicts the scaling expected if these structures are ion acoustic solitons ($\sim$ 50 λ_D, due to the artificial mass ratio), but it agrees with the size directly measured in the simulations. The potential amplitudes, $e\phi/kT_e$, for the lower beam speeds presented here are of the order of 0.1, as has been seen by Polar [*Bounds et al.*, 1999; Dombeck et al., in press, 2001]. The potential amplitude was $\sim$ 0.1 in the lowest beam energy (0.2 v_{te} - 2 keV) case presented here. For the larger beam speeds the simulated potential amplitudes ($e\phi/kT_e \gtrsim 0.1$) are somewhat larger than the typical values seen by Polar ($e\phi/kT_e \lesssim 0.1$) (Dombeck et al., in press, 2001), but the beam speeds in

those simulation runs were also greater than the Polar observations. The potential amplitudes for similar beam speeds are consistent between the simulations and the Polar data.

5. Conclusions

Recent spacecraft observations of ion solitary waves and plasma parameters in the auroral zone suggested the need to perform new simulations. When input parameters for the simulations are updated to exclude cold plasma, as determined from recent FAST observations, and include hydrogen and oxygen beams, solitary structures result which resemble the observed structures in the following ways:

1. The solitary wave speeds fall between the beam speeds of the hydrogen and oxygen beams, as would be expected if the two-stream instability was involved.

2. The structure sizes observed in the simulation are $\sim 10\ \lambda_D$ both parallel to and perpendicular to the magnetic field line. If these structures are assumed to be ion acoustic solitons, the perpendicular scale size to compare to the observations would be $\sim\ 50\ \lambda_D$, owing to the effects of the artificial mass ratio used in this study. Observations find the sizes to be of the order of $10\ \lambda_D$.

3. The potential amplitude of these ion solitary waves is similar to what has been seen in the observations, $e\phi/kT_e \sim 0.1$.

Further work needs to be done to better understand ion solitary waves in the magnetosphere. Among the unanswered questions is why ion solitary waves have only been observed in the auroral zone, while electron solitary waves have been observed in many regions. Earlier speculation that ion solitary waves were not observed at high altitudes owing to the lower ratio of Ω_e/ω_{pe} [*Cattell et al.*, 1999] has not been borne out by this study, though it is possible that differences in plasma distribution function shape explain the lack of observations of ion solitary waves in other regions. Simulations with smaller time steps and spatial scales need to be performed, in order to better see how the spatial structure of ion solitary waves evolves. Studies including He^+ and hot plasma sheet ions should be performed as well, since these populations are observed in upward beam regions. Further statistical studies of the perpendicular scale sizes of solitary structures are needed, since single-observation estimates of perpendicular scale size are difficult.

Acknowledgments. We would like to thank Victor Marchenko and Mary Hudson for giving us their simulation code and their assistance with its use. This work was supported by the NASA grants NAG5-3182, NAG5-3217, NAG5-3596, NAG5-7442, NGT5-50251, and NGT5-50293. Computing resources were provided by the Supercomputing Institute for Digital Simulation and Advanced Computation.

Janet G. Luhmann thanks Jason R. Franz and Xianyang Wu for their assistance in evaluating this paper.

References

Bale, S. D., P. J. Kellogg, D. E. Larson, R. P. Lin, K. Goetz, and R. P. Lepping, Bipolar electrostatic structures in the shock transition region: Evidence of electron phase space holes, *Geophys. Res. Lett.*, *25*, 2929–2932, 1998.

Barnes, C., M. K. Hudson, and W. Lotko, Weak double layers in ion-acoustic turbulence, *Phys. Fluids*, *28*, 1055–1062, 1985.

Bergmann, R., and W. Lotko, Transition to unstable ion flow in parallel electric fields, *J. Geophys. Res.*, *91*, 7033–7045, 1986.

Bergmann, R., I. Roth, and M. K. Hudson, Linear stability of the H^+/-O^+ two-stream interaction in a magnetized plasma, *J. Geophys. Res.*, *93*, 4005–4020, 1988.

Boström, R., G. Gustafsson, B. Holback, G. Holmgren, H. Koskinen, and P. Kintner, Characteristics of solitary waves and weak double layers in the magnetospheric plasma, *Phys. Rev. Lett.*, *61*, 82–85, 1988.

Bounds, S. R., R. F. Pfaff, S. F. Knowlton, F. S. Mozer, M. A. Temerin, and C. A. Kletzing, Solitary potential structures associated with ion and electron beams near 1 R_E altitude, *J. Geophys. Res.*, *104*, 28,709–28,717, 1999.

Cattell, C. A., J. Dombeck, J. R. Wygant, M. K. Hudson, F. S. Mozer, M. A. Temerin, W. K. Peterson, C. A. Kletzing, C. T. Russell, and R. F. Pfaff, Comparisons of Polar satellite observations of solitary wave velocities in the plasma sheet boundary and the high altitude cusp to those in the auroral zone, *Geophys. Res. Lett.*, *26*, 425–428, 1999.

Dombeck, J. P., C. A. Cattell, J. R. Wygant, F. S. Mozer, and C. A. Kletzing, A statistical study of solitary wave structure characteristics in data from the Polar satellite (abstract), *Trans. Am. Geophys. Union (EOS)*, *80 (46)*, *Fall Meet. Suppl.*, F860, 1999.

Dubouloz, N., R. Pottelette, M. Malingre, and R. A. Treumann, Generation of broadband electrostatic noise by electron acoustic solitons, *Geophys. Res. Lett.*, *18*, 155–158, 1991.

Dupree, T. H., Theory of phase-space density holes, *Phys. Fluids*, *25*, 277–289, 1982.

Ergun, R. E., C. W. Carlson, J. P. McFadden, F. S. Mozer, G. T. Delory, W. Peria, C. C. Chaston, M. Temerin, I. Roth, L. Muschietti, R. Elphic, R. Strangeway, R. Pfaff, C. A. Cattell, D. Klumpar, E. Shelley, W. Peterson, E. Moebius, and L. Kistler, FAST satellite observations of large-amplitude solitary structures, *Geophys. Res. Lett.*, *25*, 2041–2044, 1998.

Franz, J. R., P. M. Kintner, and J. S. Pickett, POLAR observations of coherent electric field structures, *Geophys. Res. Lett.*, *25*, 1277–1280, 1998.

Franz, J. R., P. M. Kintner, C. E. Seyler, J. S. Pickett, and J. D. Scudder, On the perpendicular scale of electron phase-space holes, *Geophys. Res. Lett.*, *27*, 169–172, 2000.

Goldman, M. V., M. M. Oppenheim, and D. L. Newman, Nonlinear two-stream instabilities as an explanation for auroral bipolar wave structures, *Geophys. Res. Lett.*, *26*, 1821–1824, 1999.

Gray, P. C., M. K. Hudson, W. Lotko, and R. Bergmann, Decay of ion beam driven acoustic waves into ion holes, *Geophys. Res. Lett.*, *18*, 1675–1678, 1991.

Gray, P. C., M. K. Hudson, and W. Lotko, Acoustic double layers in multispecies plasma, *IEEE Trans. Plasma Sci.*, *20*, 745–755, 1992.

Hudson, M. K., W. Lotko, I. Roth, and E. Witt, Solitary waves and double layers on auroral field lines, *J. Geophys. Res.*, *88*, 916–926, 1983.

Hudson, M. K., T. L. Crystal, W. Lotko, and C. Barnes, Weak double layers in the auroral ionosphere, in *Laser & Particle Beams*, vol. 5, pp. 295–313, Cambridge University Press, Cambridge, UK, 1987.

Koskinen, H. E. J., R. Lundin, and B. Holback, On the plasma environment of solitary waves and weak double layers, *J. Geophys. Res.*, *95*, 5921–5929, 1990.

Lotko, W., Reflection dissipation of an ion-acoustic soliton, *Phys. Fluids*, *26*, 1771–1779, 1983.

Mälkki, A., A. I. Eriksson, P.-O. Dovner, R. Boström, B. Holback, G. Holmgren, and H. E. J. Koskinen, A statistical survey of auroral solitary waves and weak double layers. 1. Occurrence and net voltage, *J. Geophys. Res.*, *98*, 15,521–15,530, 1993.

Marchenko, V. A., and M. K. Hudson, Beam-driven acoustic solitary waves in the auroral acceleration region, *J. Geophys. Res.*, *100*, 19,791–19,803, 1995.

Matsumoto, H., H. Kojima, T. Miyatake, Y. Omura, M. Okada, I. Nagano, and M. Tsutui, Electrostatic solitary waves (ESW) in the magnetotail: BEN wave forms observed by Geotail, *Geophys. Res. Lett.*, *21*, 2915–2918, 1994.

McFadden, J. P., C. W. Carlson, and R. E. Ergun, Microstructure of the auroral acceleration region as observed by FAST, *J. Geophys. Res.*, *104*, 14,453–14,480, 1999a.

McFadden, J. P., C. W. Carlson, and R. E. Ergun, Ion solitary waves and auroral ion beams (abstract), *Trans. Am. Geophys. Union (EOS), 80 (46), Fall Meet. Suppl.*, F834, 1999b.

McFadden, J. P., C. W. Carlson, R. E. Ergun, D. M. Klumpar, and E. Moebius, Ion and electron characteristics in auroral density cavities associated with ion beams: No evidence for cold ionospheric plasma, *J. Geophys. Res.*, *104*, 14,671–14,682, 1999c.

Mozer, F. S., R. Ergun, M. Temerin, C. Cattell, J. Dombeck, and J. Wygant, New features of time domain electric-field structures in the auroral acceleration region, *Phys. Rev. Lett.*, *79*, 1281–1284, 1997.

Muschietti, L., R. E. Ergun, I. Roth, and C. W. Carlson, Phase-space electron holes along magnetic field lines, *Geophys. Res. Lett.*, *26*, 1093–1096, 1999a.

Muschietti, L., R. E. Ergun, I. Roth, and C. W. Carlson, Correction to "Phase-space electron holes along magnetic field lines", *Geophys. Res. Lett.*, *26*, 1689, 1999b.

Qian, S., W. Lotko, and M. K. Hudson, Oxygen acoustic solitary waves in a magnetized plasma, *J. Geophys. Res.*, *94*, 1339–1346, 1989.

Singh, N., Electron holes as a common feature of double-layer-driven plasma waves, *Geophys. Res. Lett.*, *27*, 927–930, 2000.

Strangeway, R. J., L. Kepko, R. C. Elphic, C. W. Carlson, R. E. Ergun, J. P. McFadden, W. J. Peria, G. T. Delory, C. C. Chaston, M. Temerin, C. A. Cattell, E. Mobius, L. M. Kistler, D. M. Klumpar, W. K. Peterson, E. G. Shelley, and R. F. Pfaff, FAST observations of VLF waves in the auroral zone: Evidence of very low plasma densities, *Geophys. Res. Lett.*, *25*, 2065–2068, 1998.

Temerin, M., K. Cerny, W. Lotko, and F. S. Mozer, Observations of double layers and solitary waves in the auroral plasma, *Phys. Rev. Lett.*, *48*, 1175–1179, 1982.

Tetreault, D., Theory of electric fields in the auroral acceleration region, *J. Geophys. Res.*, *96*, 3549–3563, 1991.

Zakharov, V. E., and E. A. Kuznetsov, On three-dimensional solitons (in plasma), *Sov. Phys.–JETP*, *39*, 285–288, 1974.

C. A. Cattell, J. P. Crumley, J. P. Dombeck, R. L. Lysak, School of Physics and Astronomy, University of Minnesota, 116 Church St. SE, Minneapolis, MN, 55455. (cattell@belka.space.umn.edu; crumley@belka.space.umn.edu; johnd@belka.space.umn.edu; bob @aurora.space.umn.edu)

Received May 23, 2000; revised August 2, 2000; accepted August 17, 2000.